GRIP1 interlinks N-cadherin and AMPA receptors at vesicles to promote combined cargo transport into dendrites

Frank F. Heisler[a,1], Han Kyu Lee[a,1], Kira V. Gromova[a], Yvonne Pechmann[a], Beate Schurek[a], Laura Ruschkies[a], Markus Schroeder[a], Michaela Schweizer[b], and Matthias Kneussel[a,2]

[a]Department of Molecular Neurogenetics and [b]Morphology Unit, University Medical Center Hamburg-Eppendorf, Center for Molecular Neurobiology, 20251 Hamburg, Germany

Edited by Richard L. Huganir, The Johns Hopkins University School of Medicine, Baltimore, MD, and approved February 20, 2014 (received for review March 7, 2013)

The GluA2 subunit of AMPA-type glutamate receptors (AMPARs) regulates excitatory synaptic transmission in neurons. In addition, the transsynaptic cell adhesion molecule *N*-cadherin controls excitatory synapse function and stabilizes dendritic spine structures. At postsynaptic membranes, GluA2 physically binds *N*-cadherin, underlying spine growth and synaptic modulation. We report that *N*-cadherin binds to PSD-95/SAP90/DLG/ZO-1 (PDZ) domain 2 of the glutamate receptor interacting protein 1 (GRIP1) through its intracellular C terminus. *N*-cadherin and GluA2-containing AMPARs are presorted to identical transport vesicles for dendrite delivery, and live imaging reveals cotransport of both proteins. The kinesin KIF5 powers GluA2/*N*-cadherin codelivery by using GRIP1 as a multilink interface. Notably, GluA2 and *N*-cadherin use different PDZ domains on GRIP1 to simultaneously bind the transport complex, and interference with either binding motif impairs the turnover of both synaptic cargoes. Depolymerization of microtubules, deletion of the KIF5 motor domain, or specific blockade of AMPAR exocytosis affects delivery of GluA2/*N*-cadherin vesicles. At the functional level, interference with this cotransport reduces the number of spine protrusions and excitatory synapses. Our data suggest the concept that the multi-PDZ-domain adaptor protein GRIP1 can act as a scaffold at trafficking vesicles in the combined delivery of AMPARs and *N*-cadherin into dendrites.

Active vesicle transport regulates various cellular processes through delivery, recycling, and removal of plasma membrane proteins (1). In neurons, the rapid turnover of hundreds of synaptic molecules including neurotransmitter receptors and cell adhesion molecules is critical for synapse formation and function (2). AMPA-type glutamate receptors (AMPARs) are key players in this context, participating in excitatory transmission and long-term plasticity (the ability of individual synapses to persistently change in strength) (3, 4). Synaptic plasticity includes structural changes such as an enlargement of spines or postsynaptic densities (PSDs) and is often accompanied by an augmented trafficking of synaptic cargoes (2, 5). *N*-cadherin has been shown to critically stabilize the pre- and postsynaptic connection, both in synaptogenesis and during activity-dependent growth of synaptic contacts (6). In agreement with AMPARs and *N*-cadherin being involved in functional and structural synaptic plasticity, an interaction between their extracellular domains at the surface membrane was reported (7, 8) that stimulates presynaptic development and dendritic spine formation.

For anterograde delivery to dendritic spines, GluA2 directly interacts with the multi-PDZ-domain protein glutamate receptor interacting protein 1 (GRIP1), which in turn directly binds the kinesin motor protein KIF5 (9-12). GRIP1 is expressed in various tissues, harbors seven PDZ domains, and interacts with different transmembrane proteins underlying vesicle trafficking or membrane localization (13–16).

Here we report that through a direct interaction with GRIP1, *N*-cadherin already associates with AMPARs at KIF5C-driven vesicles. Transport adaptors are suggested to organize presorting of intracellular proteins, leading to subpopulations of transport vesicles with a unique identity.

Results

***N*-Cadherin Binds GRIP1 and KIF5C.** We screened for new interaction partners of PDZ domains 1–3 of GRIP1, using the yeast two-hybrid system. Two clones encoding amino acids (aa) 102–906 of *N*-cadherin were identified (Fig. 1*A* and Fig. S1 *A* and *B*). Deletion mutagenesis mapped PDZ2 of GRIP1 as sufficient for *N*-cadherin binding and aa775–791 of *N*-cadherin to mediate GRIP1 binding. Coimmunoprecipitation (co-IP) confirmed this interaction on expression of different fluorescent proteins (XFP)-fusion proteins in 3T3 and HEK293 cells (Fig. 1*B* and Fig. S1*C*) or by investigating endogenous protein from vesicle-enriched brain lysate (Fig. 1*C*). Because GRIP1 acts as a cargo adapter at KIF5-driven AMPAR vesicles (12), we asked whether KIF5 interacted with *N*-cadherin/GRIP1 associations. Co-IPs of either XFP-fusion proteins from 3T3 and HEK293 cells (Fig. 1*D* and Fig. S1*D*) or by using vesicle-enriched brain lysate (Fig. 1*E*) indeed detected triple association of *N*-cadherin with KIF5C and its cargo adaptor GRIP1. Accordingly, coimmunostainings in hippocampal neurons indicated colocalization of *N*-cadherin and GRIP1 in dendrites (Fig. S2*A*), with colocalization levels of ∼72% at spine and shaft synapses and ∼61–68% at nonsynaptic sites, containing various proteins in transit (Fig. 1 *F* and *G*).

Significance

Synapses form and change in response to neuronal activity, and they dynamically exchange transmembrane proteins over time. Most synaptic proteins are synthesized in the cell body and undergo long-distance vesicular transport powered by molecular motors along microtubules. Here we show that two synaptic key proteins (GluA2 and N-cadherin) are simultaneously delivered within distinct transport vesicles through motor proteins. Our data suggest that multidomain cargo adaptors tether synaptic proteins destined for the same subcellular compartment. We propose that vesicular presorting is an alternative mechanism to efficiently supply synapses.

Author contributions: F.F.H., H.K.L., and M.K. designed research; F.F.H., H.K.L., K.V.G., Y.P., B.S., L.R., M. Schroeder, and M. Schweizer performed research; F.F.H., H.K.L., K.V.G., M. Schweizer, and M.K. analyzed data; and F.F.H. and M.K. wrote the paper.

The authors declare no conflict of interest.

This article is a PNAS Direct Submission.

Freely available online through the PNAS open access option.

[1]F.F.H. and H.K.L. contributed equally to this work.

[2]To whom correspondence should be addressed. E-mail: matthias.kneussel@zmnh.uni-hamburg.de.

This article contains supporting information online at www.pnas.org/lookup/suppl/doi:10.1073/pnas.1304301111/-/DCSupplemental.

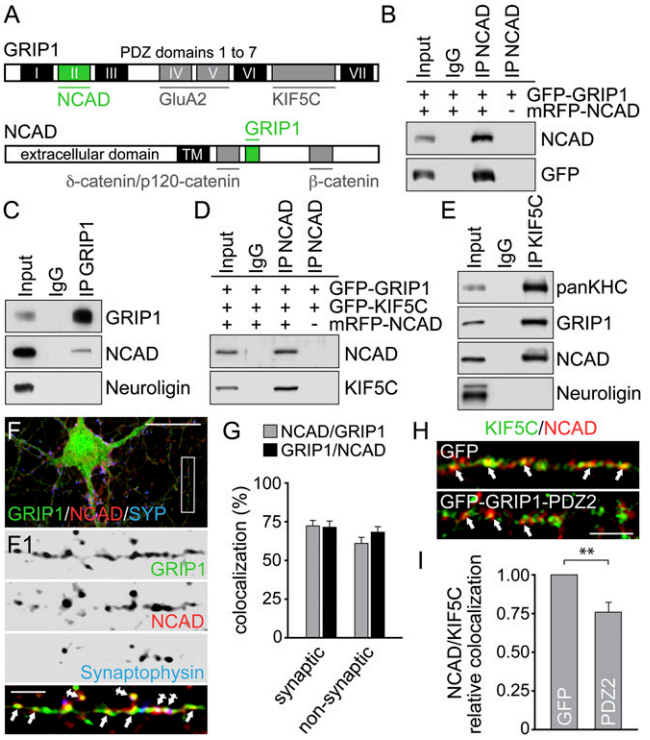

Fig. 1. *N*-cadherin binds GRIP1 and KIF5C. (*A*) GRIP1 and NCAD domain architecture. Yeast two-hybrid screening identifies PDZ2 of GRIP1 for NCAD and a C-terminal NCAD fragment for GRIP1 binding (green). Gray, previously reported binding partners. (*B–E*) Co-IPs with antibodies indicated above, detection to the right. (*B* and *D*) 3T3 cell expression. (*C* and *E*) Vesicle-enriched brain lysate. (*F* and *G*) Immunostainings of DIV15 neurons with GRIP1-, NCAD-, and Synaptophysin-specific antibodies. Arrows, nonsynaptic colocalization at dendrite shafts; crossed arrows, colocalization at spine and shaft synapses. Boxed region is shown at higher magnification. (Scale bars, 25 μm in *F* and 5 μm in *F1*.) (*G*) Synaptic colocalization: NCAD over GRIP1, 72.20 ± 3.53; GRIP1 over NCAD, 71.34 ± 3.92. Nonsynaptic colocalization: NCAD over GRIP1, 60.92 ± 3.89; GRIP1 over NCAD, 68.15 ± 3.41; 32 cells each. (*H* and *I*) Immunostaining of DIV9-12 hippocampal neurons: colocalization of NCAD/KIF5C signals (arrows; pseudocolored) is reduced on GFP-GRIP1-PDZ2 (0.77 ± 0.06; 19 cells) compared with GFP expression (set to 1; 31 cells). (Scale bar, 5 μm.) Data represent mean ± SEM. Statistical analysis, Student *t* test (***P* < 0.01).

In agreement with KIF5C mediating long-distance dendrite delivery (2), *N*-cadherin and KIF5C puncta colocalized within dendrite shafts (~52–54%) (Fig. S2 *B* and *C*), suggesting KIF5C-driven transport of *N*-cadherin-containing vesicles. Notably, KIF5C/*N*-cadherin colocalization in turn significantly decreased through competitive overexpression of the PDZ2 domain of GRIP1 that harbors the *N*-cadherin binding motif (Fig. 1 *H* and *I*). Together, this indicates that PDZ2 of GRIP1 connects *N*-cadherin to the kinesin motor protein KIF5C.

Dendrite Delivery of *N*-Cadherin and GRIP1 Depends on KIF5C. Because the trafficking of *N*-cadherin in differentiated neurons remained unclear, although activity-dependent delivery of other synaptic proteins depends on KIF5 (17), we analyzed GRIP1 and *N*-cadherin transport in neurons at later developmental stages [9 and 12 d in vitro (DIV9-12)]. Because endogenous proteins were already synaptically localized, similarly distributing XFP-fusion proteins of GRIP1 and *N*-cadherin (Fig. S3) (18, 19) were used to monitor dendrite delivery. Monomeric red fluorescent protein (mRFP)-GRIP1 and mRFP-N-cadherin (mRFP-NCAD) particles were highly delivered into dendrites in the presence of GFP-KIF5C; however, they accumulated as large clusters in the cell soma on interference with KIF5C transport, using a dominant-negative KIF5C mutant lacking the motor domain (GFP-KIF5CΔMD) (Fig. 2 *A–F* and Fig. S4 *A–F*). To test whether KIF5C also powers *N*-cadherin delivery to the plasma membrane, we labeled cell surface populations of *N*-cadherin in hippocampal neurons. Surface levels of newly synthesized mRFP-NCAD at dendrite segments were strongly increased on GFP-

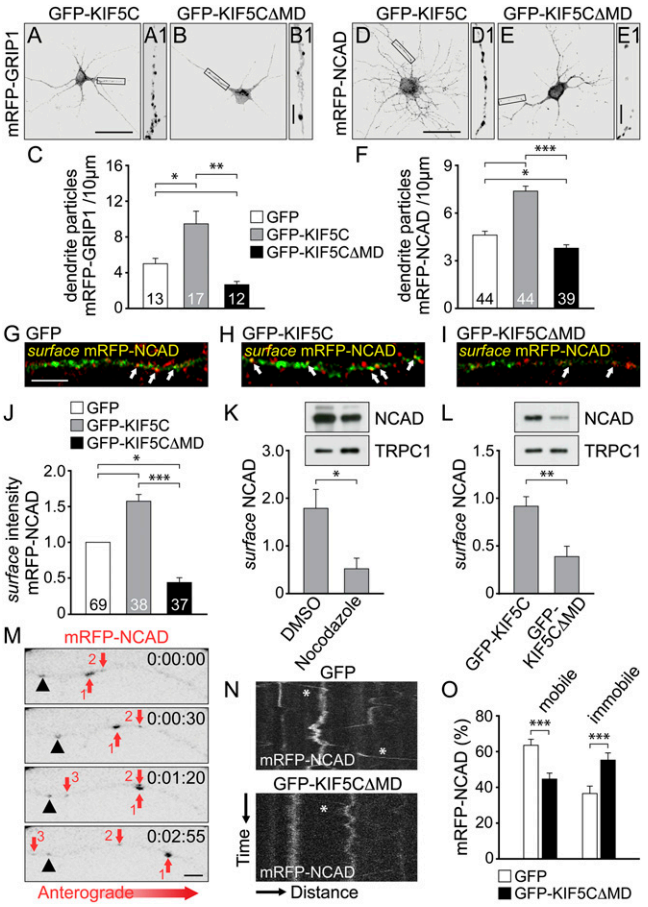

Fig. 2. KIF5C drives GRIP1 and *N*-cadherin delivery into dendrites. (*A–F*) DIV9-12 neurons (transfected with cDNAs as indicated) were analyzed for mRFP-fusion particle distribution (18 h posttransfection). Boxed regions are shown at higher magnification. (Scale bars, 50 μm in *A–E* and 5 μm in *A1–E1*). Numbers of cells as indicated. (*A–C*) Numbers of mRFP-GRIP1 dendrite particles increase on GFP-KIF5C (*A*) (9.35 ± 1.51) and decrease on GFP-KIF5CΔMD (*B*) (2.49 ± 0.35) compared with GFP coexpression (4.99 ± 0.63). (*D–F*) Numbers of mRFP-NCAD dendrite particles increase on GFP-KIF5C (*D*) (7.43 ± 0.35) and decrease on GFP-KIF5CΔMD (*E*) (3.67 ± 0.28) compared with GFP coexpression (4.44 ± 0.25). (*G–J*) Surface immunostaining of NCAD in DIV9-12 neurons 18 h posttransfection. (Scale bar, 5 μm.) Surface mRFP-NCAD signals (yellow, arrows, judged by colocalization of total mRFP-NCAD [green pseudocolor] with surface NCAD [red pseudocolor]) increase on GFP-KIF5C (*H*) (1.57 ± 0.11) and decrease on GFP-KIF5CΔMD (*I*) (0.42 ± 0.07) compared with GFP coexpression (*G*) (set to 1). Numbers of cells as indicated. (*K* and *L*) Surface biotinylation of mRFP-NCAD in HEK293 cells. Control, TRPC1. (*K*) Nocodazole lowers NCAD surface levels (0.52 ± 0.14) compared with DMSO (control, 1.77 ± 0.33) ($n = 7$). (*L*) NCAD surface levels decrease on GFP-KIF5CΔMD (0.39 ± 0.13) compared with GFP-KIF5C coexpression (0.92 ± 0.12) ($n = 6$). (*M–O*) Live imaging of mRFP-NCAD particles in DIV13-14 neurons. (*M*) Arrows 1, 2, and 3 indicate mobile particles and the arrowhead almost immobile particles. (Scale bar, 2 μm.) (*N*) Kymographs, mRFP-NCAD trajectories on GFP and GFP-KIF5CΔMD coexpression. Asterisks indicate anterograde motility. *X*-axis, 35 μm; *y* axis, 115 s. (*O*) Reduced mRFP-NCAD mobility on GFP-KIF5CΔMD (44.6 ± 4.7%) compared with GFP coexpression (63.5 ± 3.4%); immobile population: GFP (36.5 ± 3.4%) and GFP-KIF5CΔMD (55.2 ± 4.7%) ($n = 32$). Data represent mean ± SEM. Statistical analysis, Student *t* test (****P* < 0.001; ***P* < 0.01; **P* < 0.05).

KIF5C but significantly reduced after GFP-KIF5CΔMD coexpression (Fig. 2 *G–J* and Fig. S4 *G–I*). Moreover, cell surface biotinylation in HEK293 cells revealed decreased mRFP-NCAD surface levels on treatment with the microtubule depolymerizing agent nocodazole (Fig. 2*K*), indicating that intact microtubules are a prerequisite for *N*-cadherin plasma membrane delivery. In addition, GFP-KIF5CΔMD significantly reduced mRFP-NCAD surface levels (Fig. 2*L*), mimicking our observation from neurons. In video microscopy experiments, a frequent anterograde mobility of mRFP-NCAD particles over distances of several micrometers was observed (Fig. 2*M*). Notably, quantitative particle tracking revealed that GFP-KIF5CΔMD coexpression significantly decreased the level of mobile mRFP-NCAD particles, whereas it increased the immobile particle population (Fig. 2 *N* and *O* and Movies S1 and S2). Together, we conclude that the anterograde delivery of *N*-cadherin in differentiated neurons at least partially depends on KIF5C.

Vesicular AMPA Receptors and *N*-Cadherin Associate with GRIP1. KIF5C pilots GluA2-containing AMPARs into dendrites, using GRIP1 as a cargo adaptor (12). Because GRIP1 binds GluA2 through PDZ domains 4 and 5 (PDZ4,5), whereas it binds *N*-cadherin via PDZ2 (Fig. 1*A*), we asked whether the three proteins may interact simultaneously, in particular as both cargoes head for excitatory synapses.

GFP-GluA2 displayed co-IP with mRFP-NCAD from HEK293 cells (Fig. S5*A*) and endogenous GluA2 coprecipitated with *N*-cadherin and vice versa, using vesicle-enriched brain lysate (Fig. 3 *A* and *B*). Both *N*-cadherin and GluA2 also coprecipitated with GRIP1, suggesting an intracellular triple association (Fig. 3*C*). Accordingly, immunolabeling in hippocampal neurons indicated colocalization of *N*-cadherin and GluA2 in dendrites (Fig. S5*B*), with colocalization levels of ∼71–75% at spine and shaft synapses and ∼60–65% at nonsynaptic sites containing various proteins in transit (Fig. 3*D* and Fig. S5 *C* and *D*). In addition, GRIP1 puncta colocalized with *N*-cadherin/GluA2 associations within dendrite shafts (∼43–47%) (Fig. 3*E* and Fig. S5*E*). As a control, we tested the dependence of GluA2 surface delivery on KIF5C function. Similar to *N*-cadherin (Fig. 2 *J* and *L*), mCherry-KIF5CΔMD significantly reduced the amount of cell surface GluA2 in neurons (Fig. S5 *F–H*). Co-IPs therefore aimed to analyze whether GRIP1 physically connects AMPARs with *N*-cadherin. Indeed, *N*-cadherin coprecipitated significantly higher amounts of GluA2 in the presence of GFP-GRIP1 compared with GFP (Fig. 3 *F* and *G*), suggesting that the multi-PDZ domain protein GRIP1 bridges *N*-cadherin and GluA2 in the formation of a common vesicular transport complex.

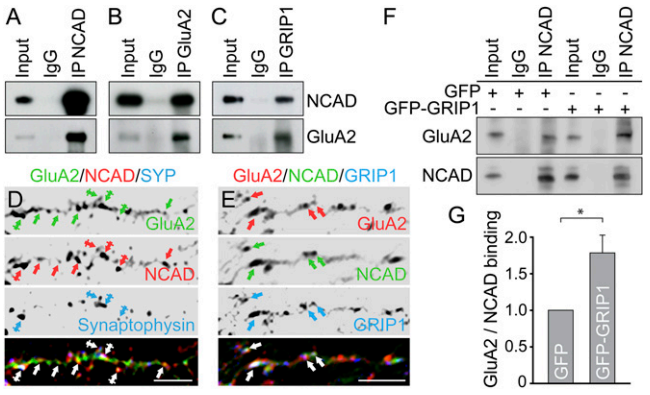

Fig. 3. GluA2 and *N*-cadherin associate through GRIP1. (*A–C*) Co-IPs from vesicle-enriched brain lysate. Antibodies for co-IPs as indicated on the top, for detection to the right. (*D* and *E*) Immunostaining in DIV15 hippocampal neurons. (*D*) Colocalization of NCAD/GluA2 at dendrite shafts (arrows, nonsynaptic) and spine or shaft synapses (crossed arrows; Synaptophysin-positive). (*E*) GRIP1 colocalizes with NCAD and GluA2 (arrows). (Scale bars, 5 μm in *D* and *E*.) (*F* and *G*) Co-IP from HEK293 cells. (*G*) GFP-GluA2 binding to mRFP-NCAD is increased on GFP-GRIP1 (1.80 ± 0.23) compared with GFP coexpression set to 1 ($n = 8$). Data represent mean ± SEM. Statistical analysis, Student *t* test (*$P < 0.05$).

Dynamic AMPA Receptor/*N*-Cadherin Transport Vesicles. To provide further evidence for a combined AMPAR/*N*-cadherin transport complex, we analyzed their occurrence at intracellular vesicles. Using electron microscopy (EM), double immunogold labeling revealed a close proximity of GluA2 and *N*-cadherin immunoreactivity not only at synapses but also at intracellular Golgi membranes and at small vesicles from both somatic and dendritic areas (Fig. 4 *A* and *B* and Fig. S6 *A–D*). Quantification of immunogold particles at Golgi near regions revealed considerable amounts (∼22–28%) of vesicles that were double-labeled for GluA2 and *N*-cadherin (Fig. 4 *A–C*). Moreover, quantitative video microscopy confirmed that ∼22% of GFP-GluA2 and mRFP-NCAD particles were cotransported in anterograde directions over distances of several micrometers (Fig. 4 *D–F* and Movie S3). In addition, we performed immunopurification of intracellular vesicles in the absence of detergent and analyzed them by EM and Western blotting (Fig. 4 *G–J*). Notably, vesicles immunoisolated with *N*-cadherin-specific antibodies harbored GluA2 within their membrane but were devoid of the cation channel transient receptor potential channel 1 (TRPC1) and Synaptophysin (used as controls). Accordingly, GluA2 was detected at *N*-cadherin-containing membranes on subsequent abrogation of protein–protein interactions through high pH treatment, which maintains the membrane integrity (Fig. 4*K*). Importantly, *N*-cadherin and GluA2 remained in physical association with GRIP1 and KIF5C when vesicle membranes were solubilized (Fig. 4*L*), indicating a common motor–cargo complex at distinct vesicle membranes. In this respect, we hypothesized that adaptor proteins such as GRIP1 can serve as multilink interfaces to specify and promote combined vesicle transport (e.g., of AMPAR/*N*-cadherin vesicles).

The Interdependence of AMPAR/*N*-Cadherin Trafficking Involves GRIP1. To test for an interdependence of both cargoes in transit and whether this involves GRIP1, we used PDZ domain fragments to compete with binding of *N*-cadherin or GluA2 to GRIP1 (Fig. 4*M*). Interestingly, a biotinylation approach revealed that overexpression of the *N*-cadherin binding site of GRIP1 (GFP-GRIP1-PDZ2) caused a significant cell surface reduction not only of *N*-cadherin but also of GluA2 (Fig. 5 *A* and *B*). Reciprocal overexpression of the GluA2 binding site of GRIP1 (GFP-GRIP1-PDZ4,5) accordingly lowered not only GluA2 but also *N*-cadherin at the cell surface (Fig. 5 *C* and *D*). To substantiate the functional relevance of the coexistence of AMPAR and *N*-cadherin at neuronal transport vesicles, we further used a peptide sequence (Pep2m) known to specifically interrupt GluA2 binding to N-ethylmaleimide-sensitive fusion protein, which is required for AMPAR exocytosis (20). Indeed, surface stainings revealed significantly reduced GluA2 signals on Pep2m overexpression compared with Pep4c (control) (Fig. 5 *E–G*). Notably, the same approach caused a similar reduction in *N*-cadherin surface levels, indicating that at least a certain population of AMPAR-containing vesicles enters the plasma membrane together with *N*-cadherin. Moreover, at the level of motor–cargo interactions, competitive interference with *N*-cadherin–GRIP1 binding through either GFP-GRIP1-PDZ2 or GFP-NCAD-dn (harboring the GRIP1 binding site of *N*-cadherin; Fig. S1*B*) lowered GluA2/KIF5C colocalization in dendrites (Fig. 5 *H* and *I*). In contrast, interference with GluA2-GRIP1 binding through either GFP-GRIP1-PDZ4,5 or GFP-GluA2-dn (harboring the GRIP1 binding site of GluA2) (9, 21) significantly reduced *N*-cadherin/KIF5C colocalization (Fig. 5 *J* and *K*). Our data suggest that the

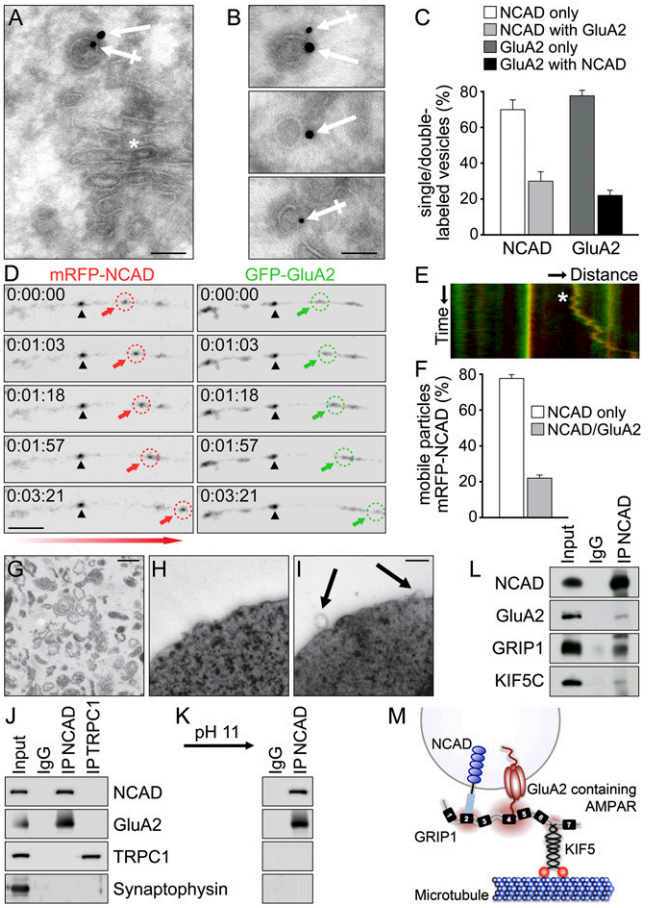

Fig. 4. GluA2 and *N*-cadherin undergo combined vesicle transport. (*A–C*) High-resolution EM of hippocampal cryosections after double immunogold labeling, using GluA2 (crossed arrows, 10 nm particles) and NCAD (arrows, 15 nm particles) antibodies. (Scale bars, 0.1 μm in *A* and *B*.) (*A*) NCAD and GluA2 signals are detected at a vesicle in proximity to Golgi membranes (asterisk). (*B*) Individual vesicle membranes are either double- or single-labeled for NCAD and/or GluA2 signals. (*C*) Quantification of single-/double-labeled vesicles at Golgi near regions: NCAD only, 71.9 ± 4.8%; NCAD with GluA2, 28.1 ± 4.8%; GluA2 only, 78.0 ± 2.7%; and GluA2 with NCAD, 22.0 ± 2.7% ($n = 17$). (*D–F*) Live imaging in DIV13-14 hippocampal neurons. (*D*) Anterograde cotransport of mRFP-NCAD and GFP-GluA2 particles along a dendrite. Arrows indicate mobile and arrowheads immobile colocalized particles. (Scale bar, 5 μm.) (*E*) Kymograph of merged particle trajectories corresponding to *D*. Asterisk indicates cotransport. *X*-axis, 25 μm; *y*-axis, 321 s. (*F*) Within a population of 1,096 mobile mRFP-NCAD particles, 78.0 ± 1.6% are negative and 22.0 ± 1.6% positive for GFP-GluA2 ($n = 37$). (*G–K*) Immunoisolation of vesicles from vesicle-enriched brain fractions. EM analysis: (*G*) vesicle fractions, (*I*) NCAD antibody-coated beads isolate vesicles (arrows), and (*H*) IgG-coated beads (control) lack membrane profiles. (Scale bars, 0.3 μm in *G* and 0.2 μm in *H* and *I*.) (*J*) Detection of GluA2 but not TRPC1 or Synaptophysin at vesicles isolated with NCAD antibodies. Vesicles isolated with TRPC1 antibodies lack GluA2, NCAD, and Synaptophysin. (*K*) GluA2 remains detected at NCAD vesicles on abrogation of protein–protein interactions (pH11 wash). (*L*) Co-IP from vesicle-enriched brain lysate on membrane solubilization. NCAD coprecipitates GluA2, GRIP1, and KIF5C. (*M*) Model of combined vesicle transport. GRIP1 interlinks NCAD (via PDZ2) and GluA2 (via PDZ4,5) while it connects cargoes to the motor protein KIF5C (via PDZ6,7).

simultaneous binding of both cargo proteins to GRIP1 facilitates their plasma membrane targeting via KIF5C-mediated vesicle transport.

Coupled AMPAR/*N*-Cadherin Trafficking Is Critical for Neuronal Connectivity. Because *N*-cadherin is critical for the development and stabilization of dendritic spines (6), we analyzed the numbers of dendritic protrusions on interference with KIF5C motor activity or after competitive interference of either GluA2- or *N*-cadherin binding to GRIP1. Using mRFP as a volume marker, neurons overexpressing GFP-KIF5CΔMD, GFP-GRIP1-PDZ2, or GFP-GRIP1-PDZ4,5 showed significantly reduced numbers of dendritic protrusions (Fig. 6 *A–E*). Together with our previous results, this suggests that AMPAR/*N*-cadherin vesicle codelivery through GRIP1/KIF5C promotes spine development.

As a consequence, the quantitative analysis of excitatory synapse numbers (represented by colocalization of presynaptic Synaptophysin and postsynaptic PSD-95) revealed a significant loss of synaptic contacts in the presence of either GFP-GRIP1-PDZ2 or GFP-GRIP1-PDZ4,5 compared with GFP (Fig. 6 *F* and *G*). In summary, we conclude that subpopulations of AMPARs and *N*-cadherin use GRIP1 as multilink interface to undergo KIF5C-driven vesicular cotransport with consequences for dendritic spine integrity and synaptic connectivity.

Discussion

N-cadherin employs a p120-catenin/KIF5C complex for transport in fibroblasts (22) and a β-catenin/KIF3 complex during neural progenitor development (23, 24). Our data show that in

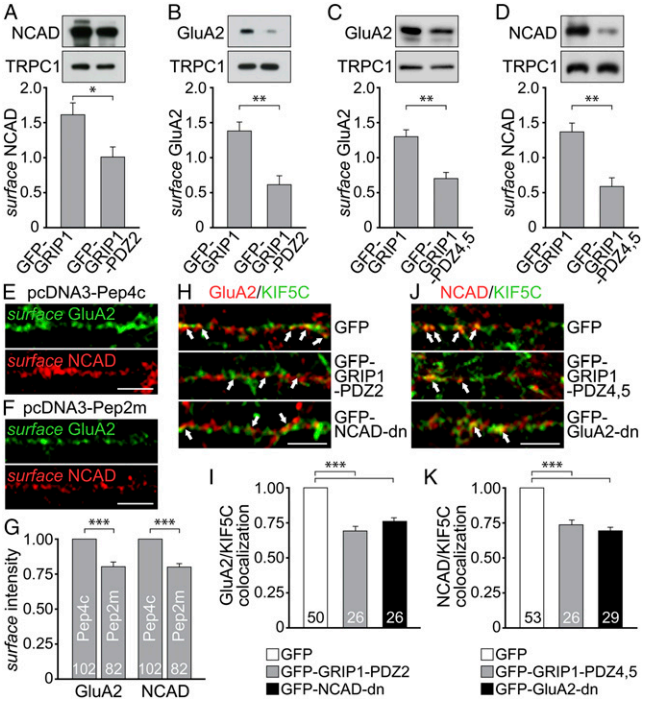

Fig. 5. GluA2 and *N*-cadherin couple GRIP1 simultaneously for efficient surface delivery. (*A–D*) Surface biotinylation of mRFP-NCAD and GFP-GluA2 in HEK293 cells. Control, TRPC1. (*A* and *B*) GFP-GRIP1-PDZ2 lowers NCAD (1.02 ± 0.15; $n = 7$) and GluA2 (0.62 ± 0.13; $n = 5$) surface levels compared with GFP-GRIP1 (1.60 ± 0.22 and 1.38 ± 0.13, respectively). (*C* and *D*) GFP-GRIP1-PDZ4,5 reduces GluA2 (0.70 ± 0.08; $n = 8$) and NCAD (0.61 ± 0.12; $n = 6$) surface levels compared with GFP-GRIP1 (1.30 ± 0.08 and 1.39 ± 0.12, respectively). (*E–G*) Surface immunostainings in DIV9-12 neurons. Reduced GluA2 and NCAD intensities (0.79 ± 0.02 and 0.78 ± 0.02) on pcDNA3-Pep2m compared with pcDNA3-Pep4c coexpression (set to 1). Numbers of cells as indicated. (Scale bars, 5 μm.) (*H–K*) Immunostaining of DIV9-12 hippocampal neurons (KIF5C pseudocolored). (*H* and *I*) GluA2/KIF5C colocalization levels (arrows) are reduced on GFP-GRIP1-PDZ2 (0.68 ± 0.02) or GFP-NCAD-dn (0.77 ± 0.02) compared with GFP expression (set to 1). (*J* and *K*) NCAD/KIF5C colocalization levels (arrows) are reduced on GFP-GRIP1-PDZ4,5 (0.74 ± 0.03) or GFP-GluA2-dn (0.69 ± 0.02) compared with GFP expression (set to 1). Numbers of cells as indicated. (Scale bar, 5 μm.) Data represent mean ± SEM. Statistical analysis, Student *t* test (***$P < 0.001$; **$P < 0.01$; *$P < 0.05$).

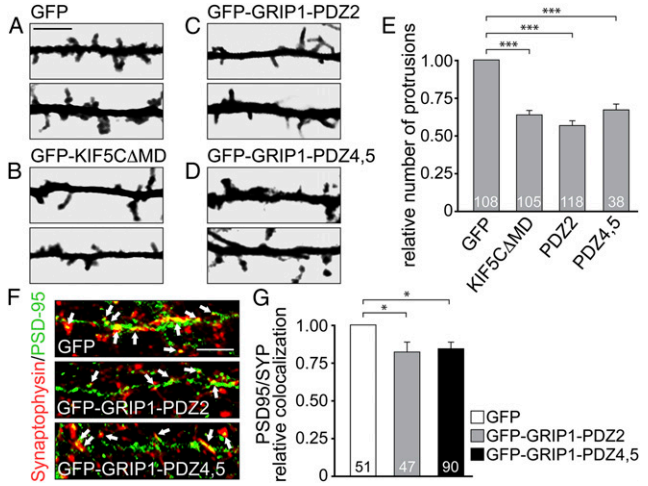

Fig. 6. Uncoupling either GluA2 or NCAD from the transport complex affects synaptic connectivity. (*A–E*) Protrusion numbers of hippocampal neurons (transfected at DIV9-12) analyzed 36 h posttransfection at distal dendrites, using a volume marker (mRFP). (Scale bar, 5 μm.) (*E*) GFP-KIF5CΔMD (0.65 ± 0.03), GFP-GRIP1-PDZ2 (0.56 ± 0.03), and GFP-GRIP1-PDZ4,5 (0.68 ± 0.04) coexpression reduces protrusion numbers compared with GFP (set to 1). Numbers of cells as indicated. (*F* and *G*) Synaptic contacts in neurons (transfected at DIV9-12) analyzed 18 h posttransfection through PSD-95/Synaptophysin coimmunostaining (PSD-95 pseudocolored). (Scale bar, 5 μm.) Compared with GFP (set to 1), GFP-GRIP1-PDZ2 (0.82 ± 0.06) and GFP-GRIP1-PDZ4,5 (0.85 ± 0.04) expression reduces the level of PSD-95/Synaptophysin colocalization (arrows). Numbers of cells as indicated. Data represent mean ± SEM. Statistical analysis, Student *t* test (***$P < 0.001$; *$P < 0.05$).

differentiated neurons, GRIP1/KIF5C is involved in the proper delivery of *N*-cadherin into dendrites. Therefore, *N*-cadherin may use alternative transport factors, depending on the developmental stage or the destined subcellular destination. In support of this, the binding sites of catenins and GRIP1 map to separate regions on *N*-cadherin.

In addition, our study reveals AMPAR/*N*-cadherin cotransport and offers mechanistic insights into its organization through the adaptor protein GRIP1. Previous studies reported that axonal trafficking organelles in general could contain multiple cargoes (25–27). TrkB, for instance, is transported with synaptic vesicle precursors to function in synapse formation (28). Other reports suggest that linker proteins connect cell adhesion molecules on the plasma membrane to intracellular transport vesicles to allow for a direct supply to nascent synapses after initial contact formation (29, 30). For example, Neuroligin1 at the cell surface is linked to NMDA receptor-containing vesicles via membrane-associated guanylate kinases and surface NCAM to post-Golgi organelles via Spectrin (29, 30). However, this cotrafficking of surface and vesicle proteins differs from the transport complex described here, which represents the trafficking of multiple cargoes within a single vesicle.

Regarding this, a recent study showed that the proper assembly of synaptic vesicle precursors requires the presence of two core components, Piccolo and Bassoon (31). Unfortunately, the molecular processes by which the multiple cargoes are selected and further linked to motor proteins to target specific subcellular destinations largely remain unknown. We suggest a mechanism by which a multi-PDZ domain protein (GRIP1) serves as a multilink interface to tether cargoes within one vesicle and to connect it to the respective motor protein. In contrast to the above-mentioned function of cotransported surface/vesicle proteins in synapse formation, intracellular codelivery of AMPAR with *N*-cadherin might represent an efficient option to approach the increasing demands of synaptic proteins during later developmental stages; however, this remains to be directly observed.

Considering that GluA2 and *N*-cadherin codelivery involves a distinct population of transport vesicles, both factors should also independently reach the cell surface in other vesicle populations. The composition of different vesicles might vary, depending on the specific needs of the acceptor compartment; for instance, during synaptic activity changes.

In this respect, AMPAR/*N*-cadherin vesicles could harbor additional cargoes such as the scaffolding molecule δ-catenin that anchors GluA2 and *N*-cadherin at synaptic sites (32). In addition, the extracellular interaction of GluA2 and *N*-cadherin (7), if it takes place inside the vesicle lumen, could strengthen the stability of the complex.

Further studies should clarify whether AMPAR/*N*-cadherin codelivery contributes to the differentiation or to plastic changes of synapses and whether it exclusively applies to post-Golgi transport or to endocytic recycling processes as well. Our data suggest that multidomain adaptor proteins play important roles in providing vesicle identity and in the combined delivery of functionally associated key molecules.

Materials and Methods

Constructs and Antibodies. All constructs were verified by dideoxy sequencing. For details on plasmids, construction of mutants, and antibodies, see *SI Materials and Methods*.

Yeast Two-Hybrid Screening. The Matchmaker LexA Yeast Two-Hybrid system (Clontech) and a rat brain cDNA library (Origene) were used for protein–protein interaction screening. Interaction of bait (pGilda) and prey (pJG4-5) fusions were assayed by activation of the *LEU2* and l*acZ* reporter genes, as previously described (33).

Cell Culture and Transfection. Primary cultures of hippocampal neurons were prepared from mice at embryonic day 16 or postnatal day 0 (P0), as described (33). Cells were transfected with a calcium phosphate coprecipitation method (33). See *SI Materials and Methods*.

Differential Centrifugation and Vesicle Immunoisolation. Whole mouse brains (P9–12) were homogenized and subjected to subsequent centrifugation steps. Antibody-coated Dynabeads M280 sheep anti mouse (Invitrogen) were used for immunopurification of vesicles (27). See *SI Materials and Methods*.

Immunocytochemistry and EM. For postembedding immunogold labeling, ultrathin cryosections (70 nm) from hippocampus were cut and labeled. CA1 hippocampal neurons were examined using a Zeiss EM 902 (Carl Zeiss). See *SI Materials and Methods*.

Surface Biotinylation Assay. Cell surface expressed molecules were labeled with biotinamido-hexanoic acid 3-sulfo-N-hydroxysuccinimid-ester (Sigma) and precipitated with Dynabeads Myone TM Streptavidin C1 (Invitrogen). See *SI Materials and Methods*.

Time-lapse Video Microscopy, Image Processing, and Statistical Analysis. During live imaging, transfected hippocampal neurons (DIV13-14) were temperature-controlled (37 °C) and CO_2-controlled. Images were acquired using Spinning Disk (Tonegawa) live cell confocal technology (Visitron Systems). Live cell confocal technology was combined with two charge-coupled device EM cameras (Hamamatsu Photonics) and equipped with an optical image splitter for simultaneous dual image acquisition. See *SI Materials and Methods*.

ACKNOWLEDGMENTS. We are grateful to M. Peckham for sharing GFP-KIF5C, P. Seeburg and D. Choquet for sharing GFP-GluA2, H. Tanaka for sharing pCXN2-N-cadherin-Venus, and R. Tsien for sharing pmRFP-N1. We thank Y. Goda, W. Wagner, and T. Hausrat for comments on the manuscript; B. Schwanke and S. Moritz for technical assistance; and M. Frotscher for advice on EM. This research was supported by Deutsche Forschungsgemeinschaft Grants KN556/4-2, KN556/6-1, and GRK1459, and by neurodapt! (to M.K.).

1. Soldati T, Schliwa M (2006) Powering membrane traffic in endocytosis and recycling. *Nat Rev Mol Cell Biol* 7(12):897–908.
2. Hirokawa N, Niwa S, Tanaka Y (2010) Molecular motors in neurons: Transport mechanisms and roles in brain function, development, and disease. *Neuron* 68(4):610–638.
3. Malinow R, Malenka RC (2002) AMPA receptor trafficking and synaptic plasticity. *Annu Rev Neurosci* 25:103–126.
4. Derkach VA, Oh MC, Guire ES, Soderling TR (2007) Regulatory mechanisms of AMPA receptors in synaptic plasticity. *Nat Rev Neurosci* 8(2):101–113.
5. Shepherd JD, Huganir RL (2007) The cell biology of synaptic plasticity: AMPA receptor trafficking. *Annu Rev Cell Dev Biol* 23:613–643.
6. Takeichi M, Abe K (2005) Synaptic contact dynamics controlled by cadherin and catenins. *Trends Cell Biol* 15(4):216–221.
7. Saglietti L, et al. (2007) Extracellular interactions between GluR2 and N-cadherin in spine regulation. *Neuron* 54(3):461–477.
8. Zhou Z, Hu J, Passafaro M, Xie W, Jia Z (2011) GluA2 (GluR2) regulates metabotropic glutamate receptor-dependent long-term depression through N-cadherin-dependent and cofilin-mediated actin reorganization. *J Neurosci* 31(3):819–833.
9. Dong H, et al. (1997) GRIP: A synaptic PDZ domain-containing protein that interacts with AMPA receptors. *Nature* 386(6622):279–284.
10. Srivastava S, et al. (1998) Novel anchorage of GluR2/3 to the postsynaptic density by the AMPA receptor-binding protein ABP. *Neuron* 21(3):581–591.
11. Wyszynski M, et al. (1999) Association of AMPA receptors with a subset of glutamate receptor-interacting protein in vivo. *J Neurosci* 19(15):6528–6537.
12. Setou M, et al. (2002) Glutamate-receptor-interacting protein GRIP1 directly steers kinesin to dendrites. *Nature* 417(6884):83–87.
13. Brückner K, et al. (1999) EphrinB ligands recruit GRIP family PDZ adaptor proteins into raft membrane microdomains. *Neuron* 22(3):511–524.
14. Takamiya K, et al. (2004) A direct functional link between the multi-PDZ domain protein GRIP1 and the Fraser syndrome protein Fras1. *Nat Genet* 36(2):172–177.
15. Hoogenraad CC, Milstein AD, Ethell IM, Henkemeyer M, Sheng M (2005) GRIP1 controls dendrite morphogenesis by regulating EphB receptor trafficking. *Nat Neurosci* 8(7):906–915.
16. Zhang J, et al. (2011) The AAA+ ATPase Thorase regulates AMPA receptor-dependent synaptic plasticity and behavior. *Cell* 145(2):284–299.
17. Cai Q, Pan PY, Sheng ZH (2007) Syntabulin-kinesin-1 family member 5B-mediated axonal transport contributes to activity-dependent presynaptic assembly. *J Neurosci* 27(27):7284–7296.
18. Thoumine O, Lambert M, Mège RM, Choquet D (2006) Regulation of N-cadherin dynamics at neuronal contacts by ligand binding and cytoskeletal coupling. *Mol Biol Cell* 17(2):862–875.
19. Maas C, et al. (2009) Synaptic activation modifies microtubules underlying transport of postsynaptic cargo. *Proc Natl Acad Sci USA* 106(21):8731–8736.
20. Beretta F, et al. (2005) NSF interaction is important for direct insertion of GluR2 at synaptic sites. *Mol Cell Neurosci* 28(4):650–660.
21. Osten P, et al. (2000) Mutagenesis reveals a role for ABP/GRIP binding to GluR2 in synaptic surface accumulation of the AMPA receptor. *Neuron* 27(2):313–325.
22. Chen X, Kojima S, Borisy GG, Green KJ (2003) p120 catenin associates with kinesin and facilitates the transport of cadherin-catenin complexes to intercellular junctions. *J Cell Biol* 163(3):547–557.
23. Teng J, et al. (2005) The KIF3 motor transports N-cadherin and organizes the developing neuroepithelium. *Nat Cell Biol* 7(5):474–482.
24. Tanuma N, et al. (2009) Protein phosphatase Dusp26 associates with KIF3 motor and promotes N-cadherin-mediated cell-cell adhesion. *Oncogene* 28(5):752–761.
25. Shapira M, et al. (2003) Unitary assembly of presynaptic active zones from Piccolo-Bassoon transport vesicles. *Neuron* 38(2):237–252.
26. Muresan Z, Muresan V (2005) Coordinated transport of phosphorylated amyloid-beta precursor protein and c-Jun NH2-terminal kinase-interacting protein-1. *J Cell Biol* 171(4):615–625.
27. Konecna A, et al. (2006) Calsyntenin-1 docks vesicular cargo to kinesin-1. *Mol Biol Cell* 17(8):3651–3663.
28. Gomes RA, Hampton C, El-Sabeawy F, Sabo SL, McAllister AK (2006) The dynamic distribution of TrkB receptors before, during, and after synapse formation between cortical neurons. *J Neurosci* 26(44):11487–11500.
29. Sytnyk V, et al. (2002) Neural cell adhesion molecule promotes accumulation of TGN organelles at sites of neuron-to-neuron contacts. *J Cell Biol* 159(4):649–661.
30. Barrow SL, et al. (2009) Neuroligin1: A cell adhesion molecule that recruits PSD-95 and NMDA receptors by distinct mechanisms during synaptogenesis. *Neural Dev* 4:17.
31. Maas C, et al. (2012) Formation of Golgi-derived active zone precursor vesicles. *J Neurosci* 32(32):11095–11108.
32. Silverman JB, et al. (2007) Synaptic anchorage of AMPA receptors by cadherins through neural plakophilin-related arm protein AMPA receptor-binding protein complexes. *J Neurosci* 27(32):8505–8516.
33. Heisler FF, et al. (2011) Muskelin regulates actin filament- and microtubule-based GABA(A) receptor transport in neurons. *Neuron* 70(1):66–81.